N- and C-Terminal Flanking Regions Modulate Light-Induced Signal Transduction in the LOV2 Domain of the Blue Light Sensor Phototropin 1 from *Avena sativa*[†,‡]

Andrei S. Halavaty and Keith Moffat*

Department of Biochemistry and Molecular Biology, The University of Chicago, 929 East 57th Street, Chicago, Illinois 60637

Received August 2, 2007; Revised Manuscript Received October 1, 2007

ABSTRACT: Light sensing by photoreceptors controls phototropism, chloroplast movement, stomatal opening, and leaf expansion in plants. Understanding the molecular mechanism by which these processes are regulated requires a quantitative description of photoreceptor dynamics. We focus on a light-driven signal transduction mechanism in the LOV2 domain (LOV, light, oxygen, voltage) of the blue light photoreceptor phototropin 1 from *Avena sativa* (oat). High-resolution crystal structures of the dark and light states of an oat LOV2 construct including residues Leu404 through Leu546 (LOV2 (404−546)) have been determined at 105 and 293 K. In all four structures, LOV2 (404−546) exhibits the typical Per-ARNT-Sim (PAS) fold, flanked by an additional conserved N-terminal turn-helix-turn motif and a C-terminal flanking region containing an amphipathic Jα helix. These regions dock on the LOV2 core domain and bury several hydrophobic residues of the central β-sheet of the core domain that would otherwise be exposed to solvent. Light structures of LOV2 (404−546) reveal that formation of the covalent bond between Cys450 and the C4a atom of the flavin mononucleotide (FMN) results in local rearrangement of the hydrogen-bonding network in the FMN binding pocket. These rearrangements are associated with disruption of the Asn414−Asp515 hydrogen bond on the surface of the protein and displacement of the N- and C-terminal flanking regions of LOV2 (404−546), both of which constitute a structural signal.

Phototropism is an ability of plants to bend toward sunlight. It was recognized as one of the remarkable phenotypes among such life-important processes as growth and development. Phototropins are flavin-based photoreceptors that regulate not only phototropism, but also chloroplast movement, stomatal opening, and leaf expansion in plants (*1*−*5*).

Phototropin 1 (phot1)[1] is composed of two N-terminal light, oxygen, voltage (LOV) domains denoted LOV1 and LOV2, and a C-terminal serine/threonine kinase domain (*6*, *7*). Heterologous expression studies have shown that phot1 undergoes autophosphorylation in response to blue light absorption. Therefore, phot1 was proposed to function as a blue-light-activated kinase (*7*). Both LOV domains of phot1 bind flavin mononucleotide (FMN) (*8*) and belong to the superfamily of the PAS domain proteins found in all kingdoms of life (*9*). LOV1 and LOV2 undergo photocycles that are characterized by formation of a covalent adduct between a conserved cysteine residue in the core domain and the C4a atom of the FMN and a photoinduced blue spectral shift (*10*−*13*). Formation of the covalent bond is a molecular switch that initiates structural changes in the FMN binding pocket, which are presumed to propagate through LOV domain(s) and ultimately to the kinase domain, where they modulate its enzymatic activity. However, the rate constants and quantum efficiencies for the photoreactions indicate that LOV1 exhibits a lower photosensitivity than LOV2 (*12*). Recent studies demonstrate that LOV1 and LOV2 play distinct roles in regulating full-length photoreceptor function (*14*, *15*). LOV2 was shown to be the predominant photoreceptor domain in phot1 that modulates light-dependent autophosphorylation of the kinase domain. The LOV1 domain has been reported to self-dimerize, whereas the LOV2 domain does not. Therefore, it was suggested that LOV1 plays role in full-length photoreceptor dimerization that can also be affected by light (*15*, *16*).

X-ray structures of isolated, short LOV domain constructs from *Adiantum capillus-veneris* (*10*, *17*) and *Chlamydomonas reinhardtii* (*18*) in their light states provided the first evidence for formation of a structurally distinct photoproduct. Although there are small structural rearrangements around the FMN, these isolated LOV domain constructs do not show extensive light-induced conformational changes in the crystal. In contrast, spectroscopic data suggest that significant structural changes in longer LOV domain constructs do occur upon formation of the initial, long-lived, covalent flavin−cysteinyl adduct in solution (*13*, *19*). Harper and colleagues (*20*, *21*) have demonstrated that an amphipathic Jα helix flanking the oat core LOV2 domain at its C-terminus does undergo structural changes upon adduct formation. Their

[†] Supported by National Institutes of Health (NIH) Grant GM036452 to K.M. BioCARS is supported by NIH Grant RR07707. Use of the Advanced Photon Source is supported by the U.S. Department of Energy, Office of Science, Office of Basic Energy Sciences, under Contract No. DE-AC02-06CH11357.

[‡] Protein Data Bank accession codes for the solved structures are 2v0u, 2v0w, 2v1a, and 2v1b.

* To whom correspondence should be addressed. Phone: +1 773-702-2116. Fax: +1 773-702-0439. E-mail:moffat@cars.uchicago.edu.

[1] Abbreviations: phot1, phototropin 1; LOV domain, light, oxygen, voltage domain; PAS domain, Per-ARNT-Sim domain; FMN, flavin mononucleotide; EDTA, ethylenediaminetetraacetic acid; CDS, cryo dark structure; CLS, cryo-trapped light structure; RDS, room-temperature dark structure; RLS, room-temperature light structure; SDS−PAGE, sodium dodecyl sulphate polyacrylamide gel electrophoresis.

10.1021/bi701543e CCC: $37.00 © xxxx American Chemical Society
Published on Web 11/15/2007 PAGE EST: 8.8

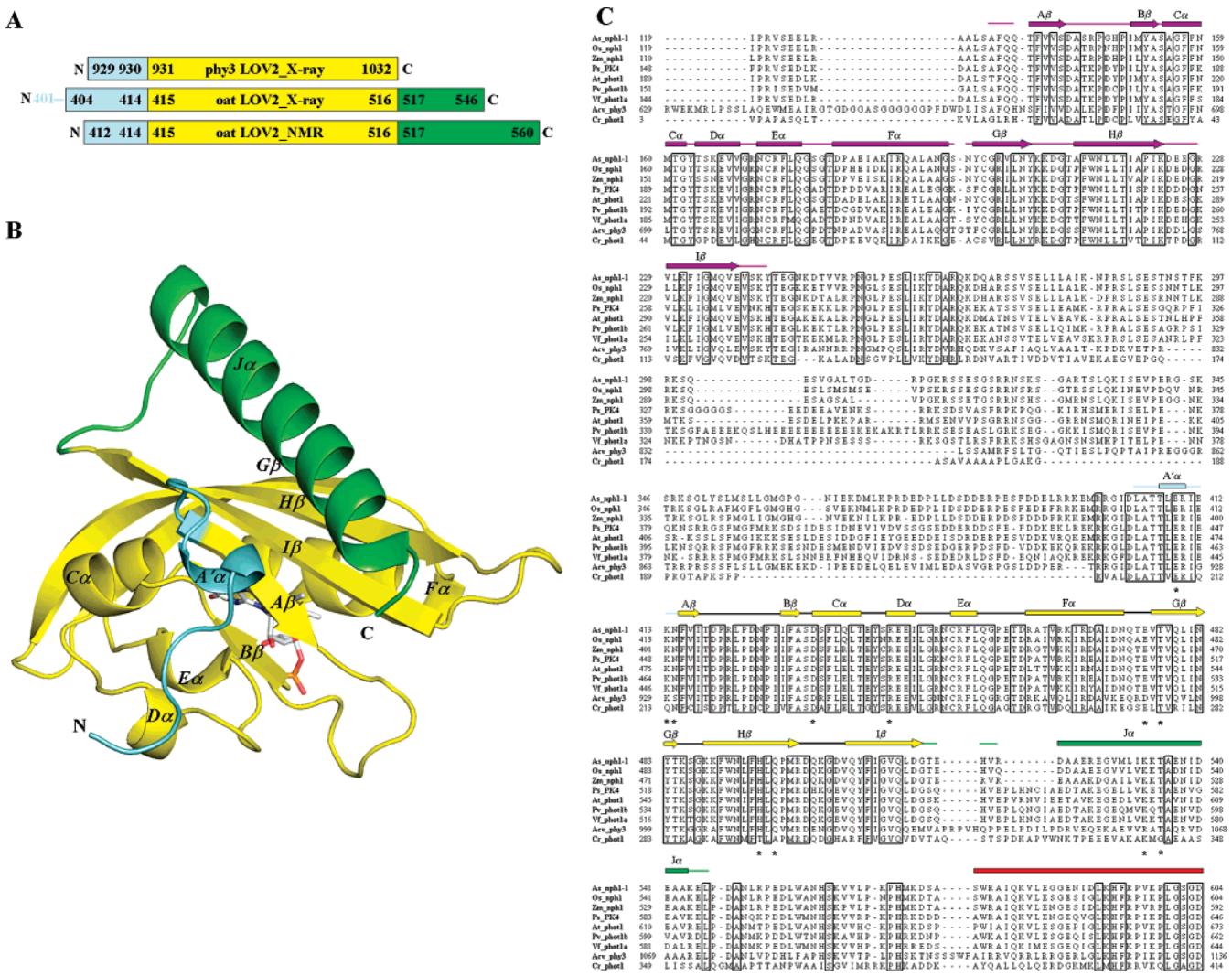

FIGURE 1: X-ray dark structure of oat LOV2 (404−546) at 1.4 Å resolution. (A) The phy3 LOV2 and two oat LOV2 constructs. The core domain is colored in yellow, N-terminal and C-terminal flanking regions in cyan and green. (B) Ribbon diagram of the dark structure of LOV2 (404−546) colored as in panel A. Secondary structure elements are designated according to the nomenclature of the PAS domain superfamily (*9*). FMN is colored by element: carbon, gray; nitrogen, blue; oxygen, red; phosphorus, orange. Figure generated with the PyMol program (*48*). (C) Sequence alignment of LOV domain proteins: *A. sativa* phot1 (O49003), *Oryza sativa* nph1 (Q9SC66), *Zea mays* nph1 (O48547), *Pisum sativa* PK4 (P93489), *A. thaliana* phot1 (O48963), *Phaseolus vulgaris* phot1b (Q5DW43), *Vicia faba* phot1a (Q8H935), *A. capillus-veneris* PHY3 (Q9ZWQ6), and *C. reinhardtii* phot1 (Q8LPE0). Sequences were aligned using the NCBI BLAST (*49*) and BioEdit (*50*) programs using accessory application ClustalW (*51*). Regions shown are LOV1 and LOV2 domains and the N-terminal part of the kinase domains. Residues with 100% sequence identity are shown in boxes. Secondary structural elements of the core LOV1 domain from *C. reinhardtii* phot1 (*18*) are shown above the LOV1 sequences and colored in magenta; secondary structural elements of LOV2 (404−546) are shown above the LOV2 sequences and colored according to panel A. The N-terminal part of the kinase domains is marked with a red box. Boundaries of the core LOV and the kinase domains are based on multiple sequence and structural alignments. Residues involved in the hydrogen-bonding network between the flanking regions and the core domain of LOV2 (404−546) are marked with an asterisk (see Figure 2A for details).

NMR and site-directed mutagenesis studies showed that destabilization of interactions between the core LOV2 domain and the Jα helix may play an important role in propagation of the initial structural signal from the photosensor domain to the output kinase domain.

We conducted X-ray crystallographic studies to explore the light-induced structural changes in the oat LOV2 (404−546) construct and, in particular, to determine whether a C-terminal flanking region containing the Jα helix plays a structural role in light-mediated signal propagation.

MATERIALS AND METHODS

LOV2 (404−546) and LOV2 (404−560) Constructs. LOV2 (404−560) construct was provided by Dr. Kevin Gardner. 5′-GAGGCGGCAAAAGAACTTTAGACTCGAGCACCACCACC-3′ and 5′-GGTGGTGGTGCTCGAGTCTAAAGTTCTTTTGCCGCCTC-3′ primers were used to eliminate 14 amino acid residues C-terminal to the Jα helix of the LOV2 (404−560) construct. The resulting LOV (404−546) construct was subcloned into the expression vector pHis-Gb1-Parallel1 as described (*20*). Construct design introduced three additional N-terminal residues, Gly401 through Phe403, which remained in the sequence of oat LOV2 (404−546) after affinity tags were removed (Figure 1A). For clarity, we denote our LOV2 construct as LOV2 (404−546), since these residues belong to the LOV2 sequence.

Expression and Purification of Proteins. Expression and purification procedures were identical for both LOV2

constructs. *E. coli* BL21(DE3) cells containing pHis-Gb1-Parallel1 vector with a desired construct were grown at 37 °C to OD_{600} = 0.6−0.7. Expression was carried out in the presence of 1 mM isopropyl β-D-galactoside at 16 °C in the dark overnight. Induced cells were spun, resuspended, and lysed by sonication in 20 mM Tris/HCl, pH 7.4, 20 mM sodium chloride (buffer A) containing protease inhibitors EDTA-free cocktail tablet (Roche Diagnostic GmbH, Mannheim, Germany). Soluble fraction and pellet were separated by centrifugation at 4 °C, 20 000 rpm for 30 min. His-tagged proteins were eluted from an immobilized metal affinity Talon resin (Co-TALON, Clontech Laboratories, Inc., CA) with 250 mM imidazole in buffer A. Proteins were dialyzed overnight at 4 °C and then treated with AcTEV protease (Invitrogen, CA) to remove the 6His-tag and streptococcal protein G b1 domain. Cleavage was carried out at room temperature for 48 h in the dark. Cleaved and noncleaved proteins were then purified by immobilized metal affinity chromatography. Finally, cleaved products were purified on a Superdex 200 column (GE Healthcare, Uppsala, Sweden) in 20 mM Tris/HCl pH 7.4, 20% glycerol (buffer B). The extent of cleavage and final purity were analyzed by SDS−PAGE. Concentration of the proteins was determined using an extinction coefficient provided by Salomon et al. (*12*).

Light-Induced Spectral Changes of Oat LOV2 in Solution and Crystals. The photocycle of both LOV2 (404−546) and LOV2 (404−560) was investigated at 293 and 283 K in buffer B. Temperature control was maintained by a water bath (NESLAB Instruments Inc., Newington, NH). Absorption spectra were collected using a diode array spectrophotometer 8452A (Hewlett-Packard). A light-induced steady state was reached by illumination of samples for 5 s by a Xe lamp (Oriel Instruments, Stratford, CT). A UV34 filter with 340 nm cutoff was used to prevent transmission of the UV light. Dark state recovery kinetics was monitored for 760 s through changes in the absorbance at 450 nm.

Absorption measurements in crystals at room temperature (293 K) were carried out at BioCARS, Advanced Photon Source (APS), Argonne National Laboratory (ANL). The 50 × 50 × 10 μm^3 crystals of LOV2 (404−546) in MiTeGen loops (Microtechnologies for Structural Genomics, Ithaca, NY) were illuminated for 1 min with a Fostec Ace 150 W illuminator (SCHOTT North America Inc., Auburn, NY) via an optical fiber, with an output of ∼0.5 mW and ∼1 mm beam diameter at the sample. Optical spectra were recorded using a single-crystal microspectrophotometer (*22*) with a weak monitoring light and a diode array detector (Ocean Optics, Dunedin, FL) for multiwavelength measurement.

Crystallization of LOV2 (404−546). Protein was concentrated in buffer B using a centrifugal filter device (Millipore Corporation, Billerica, MA) with 5.0 kDa cutoff. Crystals of LOV2 (404−546) (14−20 mg/mL) were grown in the dark in 3 μL hanging drops at 14 and 20 °C by the vapor diffusion technique against 0.07 M sodium acetate, pH 4.6, 5.6% PEG 4000, 30% glycerol. Crystals (50 × 50 × 10 to 200 × 200 × 50 μm^3) appeared within 1 week.

Data Collection and Structure Determination. X-ray diffraction data were collected using 0.9 Å radiation at 105 K and room temperature (293 K) at the 14 BM-C beamline, BioCARS, APS, ANL. For dark and light data collection at cryogenic temperature, crystals at room temperature were flash frozen in liquid nitrogen, in the dark and after 1 min illumination with the Fostec Ace 150 W fiber optics illuminator, respectively. Room-temperature dark and light data sets were collected using the same crystal with 1 s X-ray exposure time per single frame, in which the dark data set was collected first. For the light data set, crystals were continuously illuminated with the Fostec ACE 150 W illuminator using the same setup described for the microspectrophotometer measurements. To minimize X-ray radiation damage at room temperature, several additional light data sets were collected, each on a fresh crystal (no dark data sets were collected on these crystals).

Data processing, scaling, and conversion of intensities to structure factor amplitudes were carried out with HKL2000 (*23*). The initial cryo dark structure (CDS) of LOV2 (404−546) was solved by molecular replacement using AMoRe (*24*) and the dark structure of phy3 LOV2 as a model (Protein Data Bank (PDB) entry 1G28 (*17*)). Modeling of the N- and C-terminal flanking regions, substitution of single residues in the model, and analysis of the refinement results were carried out with the Crystallographic Object-Oriented Toolkit (Coot) (*25*). The structure was refined with the program Refmac (*26*) to 1.4 Å resolution. Grouped TLS refinement produced the final CDS that we used as a search model for determination of the cryo-trapped light structure (CLS), room-temperature dark structure (RDS), and room-temperature light structure (RLS). All four structures were validated with PROCHECK (*27*, *28*) and WHAT_CHECK (*29*). Crystallographic data and refinement statistics are summarized in Table 1. Superpositions of the structures were carried out with the programs LSQKAB (*30*) and DaliLite (*31*). Intermolecular contacts were determined using the NCONT program of the ccp4i suite (*32*).

RESULTS

Dark Structure of Oat LOV2 (404−546) at 105 K. The overall structure of LOV2 (404−546) at 1.4 Å resolution adopts the PAS fold (*9*) containing the PAS core (Aβ, Bβ, Cα, Dα, and Eα), helical connector (Fα), and β-scaffold (Gβ, Hβ, and Iβ) (Figure 1B). Aβ, Bβ, and β-scaffold form a twisted five-stranded antiparallel β-sheet that together with the helices and loops of the LOV2 domain buries the isoalloxazine ring of noncovalently associated FMN from solvent but leaves the ribityl-phosphate site of the cofactor solvent-exposed (Figure 1B). The FMN binding pocket is polar on the pyrimidine side of the isoalloxazine ring and ribityl-phosphate side (Supporting Information, Figure S1) and nonpolar around the dimethylbenzene moiety. Cys450 in the flavin pocket has two side-chain conformations as in the LOV1 structure (*18*). The Sγ atom in the preferred conformation (>90%) is close to C5a (3.54 Å), N5 (3.92 Å), and C4a (4.54 Å) atoms of the FMN, and we denote it as the "dark conformation" (Figure S1). The Sγ atom of the less occupied conformation (<10%) is close to N5 (3.59 Å) and C4a (3.73 Å), and we denote it as the "light conformation" (Figure S1). The conformations differ by rotation of ∼70° about the Cα−Cβ bond. A water molecule is located close to the Sγ atom (3.55 Å) of Cys450 in the "dark conformation" (Figure S1).

The N-terminal residues Leu404 through Asn414 form a turn-helix-turn motif. Sequence alignment among phototropins and phototropin-like proteins reveals complete sequence

Table 1. Crystallographic Data and Refinement Statistics of All Four Crystal Structures, Determined in the $P2_12_12_1$ Space Group[a]

	CDS (2v0u)	CLS (2v0w)	RDS (2v1a)	RLS (2v1b)[b]
		Diffraction Data		
a, *b*, *c* (Å)	35.549 56.129 66.778	35.565 56.021 66.507	35.706 57.155 67.395	35.919 57.169 67.228
resolution (Å), overall/last shell	50−1.4/ 1.45−1.4	50−1.7/ 1.76−1.7	15.83−1.65/ 1.69−1.65	16.12−1.55/ 1.59−1.55
observations/unique reflections	179912/26704	50154/15021	57554/16777	69216/19930
R_{merge} (%), overall/last shell[c]	5.3/53	4.3/36	4.3/21	4.1/55
completeness (%), overall/last shell	100/99	98/93	97/99	96/96
$I/\sigma(I)$, overall/last shell	36/3.7	27/3.3	30/5.4	29/2.4
redundancy	6.7	3.3	3.4	3.5
		Refinement Statistics		
protein molecules/ atoms (non-hydrogen atoms)	1/1270	1/1259	1/1234	1/1261
water molecules	164	159	141	129
R_{cryst}/R_{free}, (%)[d,e]	16.5/19.6	16.0/21.5	15.6/19.5	16.4/21.2
mean B value (overall, Å^2)[f]	13.2	13.4	17.0	16.9
rmsd bonds/angles, (Å/deg)	0.009/1.293	0.016/1.553	0.010/1.250	0.014/1.634
		Ramachandran Distribution		
most favored (%)	93.9	92.4	93.8	94.6
allowed (%)	5.3	6.8	5.4	4.6
generously allowed (%)	0.8	0.8	0.8	0.8
outside allowed (%)	0.0	0.0	0.0	0.0

[a] PDB ID for each structure is shown in parentheses. [b] Data from a crystal not used for room-temperature dark data collection. [c] $R_{merge} = \sum_{hkl}\sum_i|I_i - \langle I\rangle|/\sum_{hkl}\sum_i I_i$ are given for all data and the highest resolution shell. [d] $R_{cryst} = \sum_{hkl}||F_{obs} - F_{calc}||/\sum_{hkl}|F_{obs}|$, includes all data. [e] R_{free} with 5% of randomly chosen reflections. [f] Mean B value is defined as the mean crystallographic temperature factor.

identity within this motif (Figure 1C). Residues Thr407 through Arg410 adopt a single turn of α helix that we denote as A′α (Figure 1B). The side chains of the conserved residues Glu409, Lys413, and Asn414 stabilize the N-terminal motif (Figure 2A). Moreover, Leu408 and Ile411 of the motif face the hydrophobic residues of the Aβ strand (Phe415 and Ile417), Bβ strand (Ile428 and Phe429), and the C-terminal end of the Jα helix (Ile539, Ala542, Ala543, and Ile546), thus forming a hydrophobic core close to the C-terminus (Figure 2B).

The C-terminal flanking region of LOV2 (404−546) involves the Iβ−Jα loop (residues Thr517 through Arg521) and the 33 Å long Jα helix (residues Asp522 through Lys544). Surprisingly, the entire region and in particular the Jα helix have very low sequence identity among LOV2 domains of phototropin and phototropin-like proteins (Figure 1C). However, the C-terminal end of the helix starting from Lys533 is less diverse in sequence than the N-terminal end of the helix and the Iβ−Jα loop. The amphipathic character of the Jα helix allows it to fold above the β-sheet, next to the N-terminal turn-helix-turn motif. Such docking of the helix is also consistent with NMR data (*20*). The Jα helix in both the X-ray and NMR structures is of almost the same length, but differs in geometry (Figure 2C). In the crystal structure it is straight, whereas in the NMR structure it is bent around residues Lys533 through Ala536. Two residues from this region in the crystal structure, Lys533 and Thr535, anchor the Jα helix to the core LOV2 domain and to the N-terminal turn-helix-turn motif, respectively (Figure 2A). Moreover, Glu475, Thr477, His495, Gln497, and Lys533 form an extensive hydrogen-bonding network between the core LOV2 domain and the Jα helix (Figure 2A). That is, the N-terminal turn-helix-turn motif and the C-terminal Jα helix, both flanking the LOV2 core domain, interact directly with each other and with the core domain.

Light-Driven Covalent Flavin−Cysteinyl Adduct Formation in Solution and Crystals. Illumination of LOV2 (404−546) and LOV2 (404−560) in solution induces bleaching at 450 nm and a blue shift of the absorption spectrum, generating a species that absorbs maximally at 390 nm (Supporting Information, Figure S2). This spectral intermediate has been assigned to the covalent flavin−cysteinyl adduct (*33*). The adduct breaks down spontaneously and returns to its dark state in a first-order, temperature-dependent reaction with the rate coefficients of 1.6×10^{-2} s^{-1} (at 293 K) and 6.9×10^{-3} s^{-1} (at 283 K) for LOV2 (404−546) and 2.1×10^{-2} s^{-1} (at 293 K) and 7.9×10^{-3} s^{-1} (at 283 K) for LOV2 (404−560). Crystallization of LOV2 (404−546) did not affect its spectroscopic and kinetic properties: bleaching at 450 nm and the blue spectral shift were also retained upon illumination of the crystal. LOV2 (404−546) exhibited a fully reversible photocycle in the crystal with the rate coefficient of 6.2×10^{-3} s^{-1} (at 293 K), comparable to the rate coefficient measured in solution.

Comparison of the Dark and Light Structures of LOV2 (404−546). Prolonged X-ray exposure times (5−7 s per frame) and use of small crystals resulted in ∼60−70% retention of the covalent bond between the C4a atom of the FMN and Cys450 in CLS, accompanied by ∼20−30% radiation damage of the bond due to X-ray absorption (Supporting Information, Figure S3). Decreasing the exposure time and use of bigger crystals increased retention of the covalent bond to greater than 90% in RLS (Figure S3). The existence of the "dark conformation" (<10%) in both CLS and RLS could be assigned to either an unreacted dark state or to recovery of the light state. Radiation damage caused

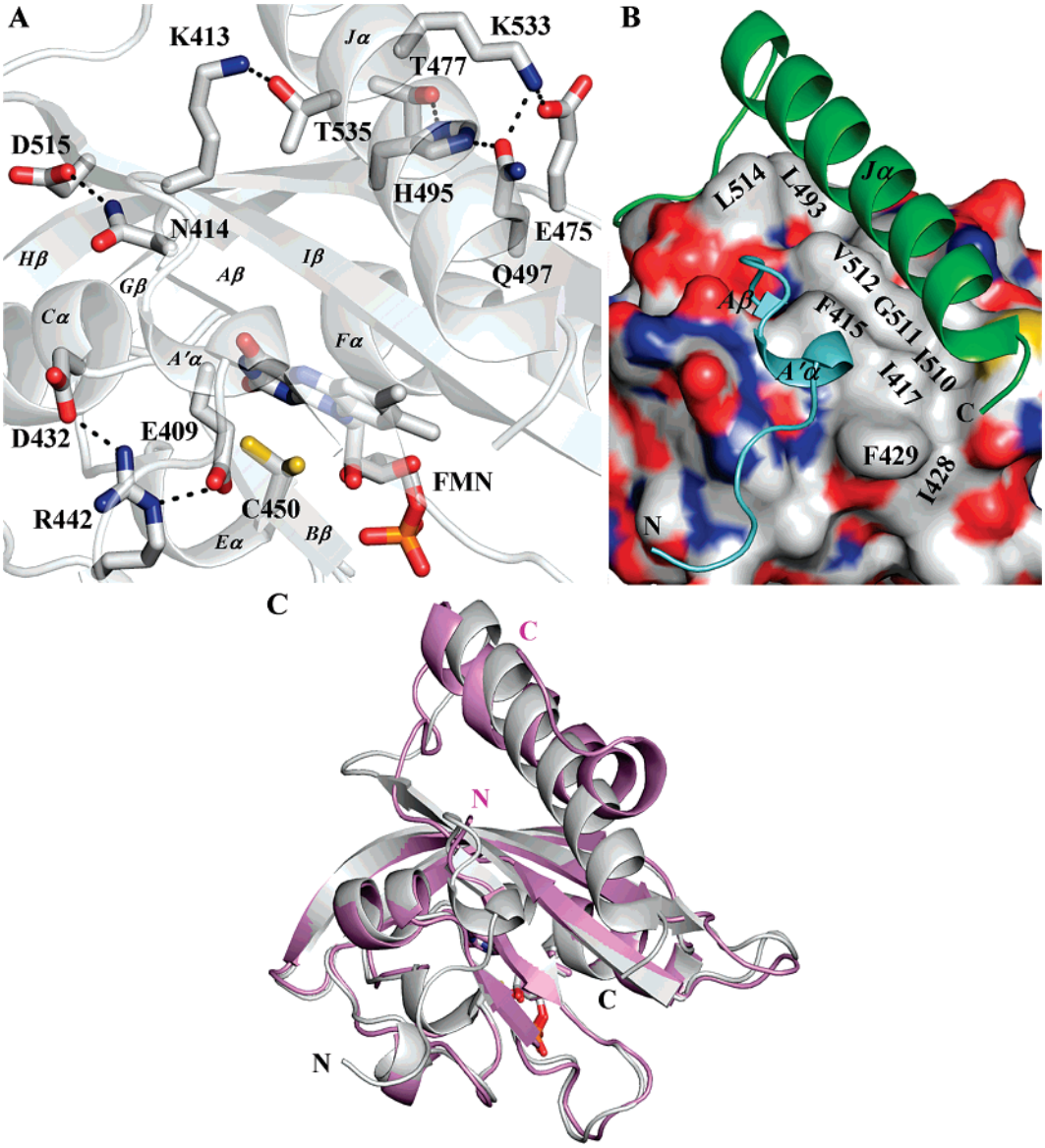

FIGURE 2: Interaction sites between the core domain and the N- and C-terminal flanking regions in the dark structure of LOV2 (404−546). (A) Residues of the N-terminal turn-helix-turn motif, the Jα helix, and the core of the LOV2 domain that are involved in intramolecular polar contacts are shown in stick representation and colored by element: carbon, gray; nitrogen, blue; oxygen, red. Hydrogen bonds are shown as black dashed lines. (B) Docking of the A′α and Jα helices on a hydrophobic patch of the core of the LOV2 domain. The core domain is shown in surface representation with atoms colored by element. The N- and C-terminal flanking regions are shown as ribbons and colored as in Figure 1B. Hydrophobic residues of the terminal helices are not shown. (C) Ribbon diagram of the superposed X-ray dark structure of LOV2 (404−546) (gray) and NMR dark structure of LOV2 (404−560) (magenta). The long, unstructured C-terminal tail of LOV2 (404−560) is not shown, and the sequence of LOV2 (404−560) is terminated at residue Leu546. Figures prepared with the PyMol program (*48*).

breakage of the bond in CLS and resulted in an appearance of a third "broken conformation" (Figure S3). Thus, determination of CLS and RLS confirmed the formation of the covalent flavin−cysteinyl adduct suggested by our spectroscopic findings in solution and in the crystals.

Upon illumination, the side chain of Cys450 rotates by ∼95° about the Cα−Cβ bond from the "dark conformation" and the thiol forms a covalent bond with C4a of the FMN. The isoalloxazine ring is no longer planar; it tilts by ∼7.0° and is displaced toward Gln513 (Figure S3). Displacement of the FMN leads to local structural rearrangements in the FMN binding pocket with the largest at Ile427, Asn449, Arg451, and Gln513. However, these structural changes have minimal effect on the overall structure and structure of the core domain of LOV2 (404−546) (Figure 3A). Comparison of CDS with CLS and RDS with RLS reveals only 0.224 and 0.200 Å overall root-mean-square deviation (rmsd) in the positions of their main chain atoms, respectively (Supporting Information, Table S1). Least-squares fitting of residues 415 through 516 that constitute the core LOV2 domain of CDS and CLS reveals an rmsd of 0.204 and 0.183 Å between RDS and RLS. That is, the structural changes in the core domain upon illumination are almost entirely small in magnitude.

Structural changes in CLS and RLS do occur on the protein surface close to the hydrophobic core formed by hydrophobic residues of the A′α helix, Aβ and Bβ strands, and the C-terminal end of the Jα helix. In this region,

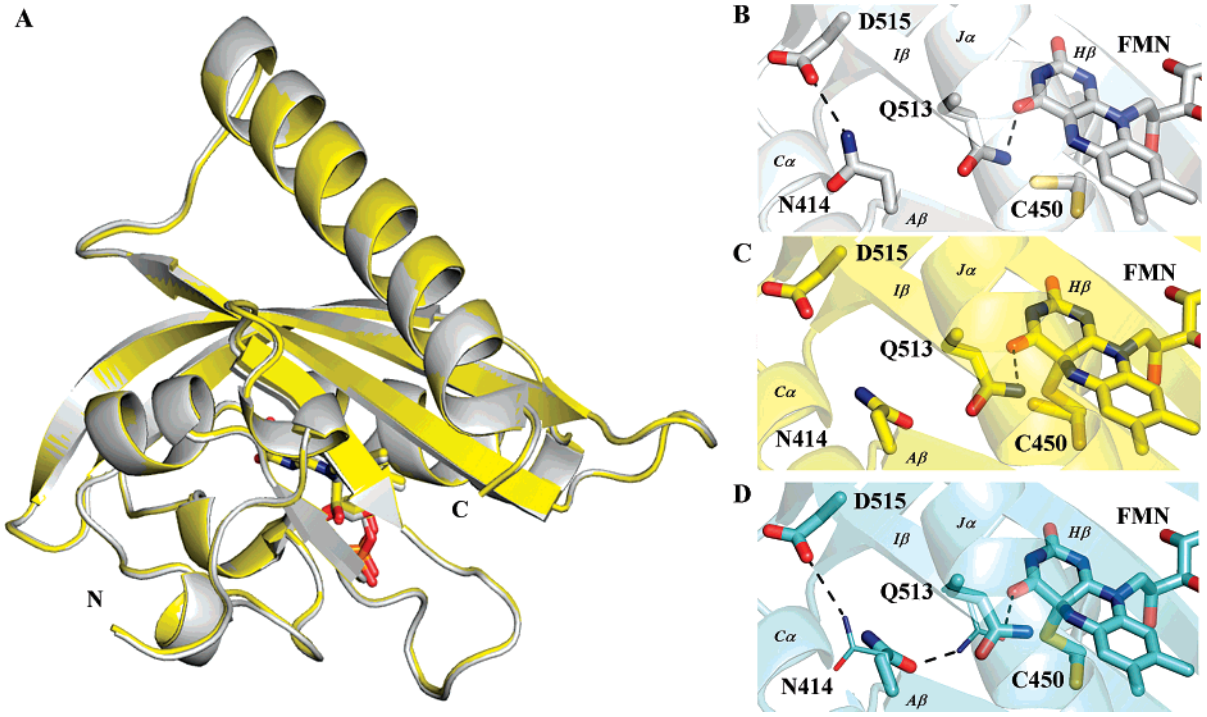

FIGURE 3: Light-induced structural changes in LOV2 (404−546). Least-squares superposition of the main chain atoms of CDS (gray) and CLS (yellow) (panel A). For rmsd between these structures see Table S1 in the Supporting Information. The vicinity of the FMN binding pocket in CDS (panel B), CLS (panel C), and RLS (panel D). The Asn414−Asp515 hydrogen bond (shown as a dashed line) observed in CDS breaks after formation of the Cys450−FMN covalent bond in CLS and RLS. Side-chain conformations of Cys450 are shown as in Figures S1 and S3 in the Supporting Information. Figures prepared with the PyMol program (*48*).

displacements of the middle part of the Jα helix, the A′α−Aβ loop, and the Aβ strand are caused by light-dependent rupture of the Asn414−Asp515 and Lys413−Thr535 hydrogen bonds present in CDS (Figure 2A and Figure 3B−D). However, the latter hydrogen bond is absent in RDS but is present in RLS. Interestingly, Asn414 in RLS has a second, minor (<40%) conformation that is represented by a single conformation of this residue in both CDS and RDS (Figure 3B−D). Moreover, Gln513 in RLS has also two conformations (Figure 3D). The hydrogen-bonding network of Glu409, Asp432, and Arg442 remains intact in both CLS and RLS (Figure 2A), and Lys533 maintains polar contacts with Glu475 and Gln497 (Figure 2A). These interactions prevent further displacement of the Jα helix and the N-terminal turn-helix-turn motif.

Examination of crystal packing showed that both the N- and C-terminal segments of LOV2 (404−546) are involved in intermolecular contacts (Figure 4A). These contacts may hinder more extensive displacement of the N-terminal motif and the Jα helix in the light structures. Nevertheless, dark minus light difference Fourier maps (CDS − CLS and RDS − RLS) show that the structural changes on the surface of the protein noted above are the most prominent (Figure 4B) and are associated with breakage of the Asn414−Asp515 hydrogen bond (Figure 3B−D). We thus propose a possible scenario for signal propagation that is similar to that reported earlier (*20*, *21*, *34*, *41*, *42*): initial, light-dependent structural changes in the FMN binding pocket propagate across the β-sheet to the hydrophobic interface formed by the core domain, the N-terminal turn-helix-turn motif, and the Jα helix (Figure 4B).

DISCUSSION

Flanking Regions of Oat LOV2 (404−546). The X-ray dark and light structures of the LOV (404−546) domain reveal a new structural N-terminal turn-helix-turn motif outside the core of the LOV2 domain adjacent to and interacting with the previously identified C-terminal Jα helix (*20*). In all four structures, the N- and C-terminal flanking regions pack against the surface of the β-sheet of the core LOV domain, stabilized both by their amphipathic character and a conserved hydrogen-bonding network among residues of these regions and the core domain (Figure 1B and Figure 2, parts A and B). LOV2 domains from phototropins have striking sequence identity within the N-terminal turn-helix-turn motif but show a much less conserved character within the C-terminal flanking region involving the amphipathic Jα helix (Figure 1C). Nevertheless, the obvious amphipathic character of these terminal regions in LOV2 domains from other phototropins (Supporting Information, Figure S4) suggests a similar structural organization to that in the oat phot1 LOV2. Such terminal helices appear to be a frequent feature of single PAS proteins and those PAS domains in multidomain proteins that are adjacent in sequence to an output (effector) domain (*20*, *21*, *34*−*42*). Might LOV1 domains in phototropins also have helical regions flanking the core domain? To date, the only X-ray structure of a core LOV1 domain is that of a short construct from *C. reinhardtii* phot1 (*18*), lacking both the N-terminal and C-terminal regions. Multiple sequence alignment of the oat LOV2 (404−546) domain and LOV1 domains from the proteins shown in Figure 1C reveals sequence identities only within the core LOV domains (Figure S4). Nevertheless, regions outside the core LOV1 domain in sequence alignment of the full-length

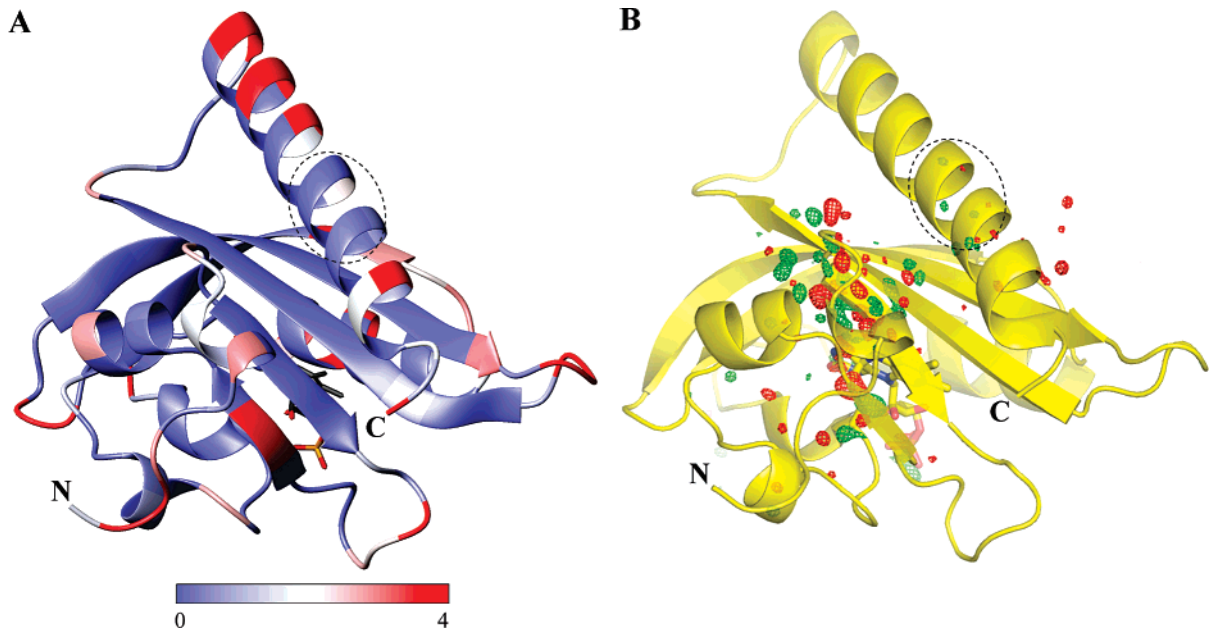

FIGURE 4: Crystal packing and signal propagation. (A) Intermolecular contacts with each residue are color-coded based on how many atoms from symmetry mates are found within a 5 Å radius, normalized by the number of atoms in that residue. The dashed oval region (residues Lys533 through Ile539) (also in panel B) highlights the middle of the Jα helix, which is not involved in crystal packing. Figure prepared with the MolMol program (*52*). (B) Dark minus light difference Fourier map (CDS − CLS) contoured at ±4σ. Positive (green) and negative (red) difference density maps identify significant structural changes in LOV2 (404−546). Figure generated with the PyMol program (*48*).

proteins (Figure 1C) tend to show amphipathic character (Figure S4) and a modest level of sequence identity. Secondary structure prediction for LOV1 domains (Figure S4) suggests that both the N- and C-terminal regions have helical structural elements.

There may be some structural/functional relationship between these helices and the presence of a hydrophobic patch on the surface of the central β-sheet of the core domain. This patch is a distinct feature, frequently observed in other PAS domains (*17*, *18*, *34*−*36*) and formed by the hydrophobic residues of the first two and the last β strands of the core domain. In LOV2 (404−546) structure these strands are Aβ, Bβ, and Iβ (Figure 2B). On the basis of structural analysis of other PAS domains (data not shown), terminal amphipathic helices can dock on the hydrophobic patch and protect it from exposure to solvent (present paper, *34*, *35*). If the structure lacks such helices, then two molecules from the same (phy3 LOV2, *17*) or different asymmetric units (*C. reinhardtii* LOV1, *18*) dock on each other and protect the patches from solvent.

Although both LOV1 and LOV2 domains do undergo photocycles in full-length phototropins, an active LOV2 domain alone is both necessary and sufficient to mediate light-dependent autophosphorylation and to establish phototropic curvature in *Arabidopsis thaliana* (*14*, *43*). Harper and colleagues (*20*, *21*) proposed a possible mechanism by which the amphipathic C-terminal Jα helix of the LOV2 domain can mediate autophosphorylation of the kinase domain in *Avena sativa* phot1. In contrast, Salomon et al. (*15*) suggest a role for LOV1 in dimerization, but not in autophosphorylation, of the native *A. sativa* phot1 in solution. Structural evidence involving N-terminal amphipathic helices in dimerization of single PAS domains was recently suggested (*34*, *35*, *37*−*39*). These helices have less sequence identity among proteins from different origins, vary in length, and dock on the hydrophobic patch noted above and contribute to the dimerization interface of those PAS domains (*35*). That is, terminal helices in LOV1 domains could be involved in full-length receptor dimerization in a manner similar to that in other structures of single PAS domains and hence control sensitization/desensitization of phot1 (*16*). However, the existence and possible role of predicted terminal helices in LOV1 domains (Figure S4) must be investigated further.

Initial Light-Induced Structural Switch in Oat LOV2 (404−*546).* Harper and colleagues (*20*, *21*) identified light-sensitive conformational changes in the C-terminal Jα helix of the oat LOV2 (404−560) construct and proposed that these changes modulate kinase activity. This hypothesis was recently supported by nanosecond time-resolved optical rotatory dispersion spectroscopy experiments on the oat LOV2 (404−559) construct that revealed a previously unobserved intermediate species (*44*). This species is characterized by a partially unfolded secondary structure, presumably localized to the Jα helix. Our crystallographic data bear on this. Structural changes originate in formation of the Cys450−FMN covalent bond and the light-induced rearrangement of hydrogen bonds in the FMN binding pocket. They propagate to both the N-terminal and the C-terminal flanking regions of oat LOV2 (404−546), not just to the C-terminal Jα helix.

A conserved glutamine residue in the FMN binding pocket was suggested to be responsible for an initial, local structural response that is further transmitted to the surface of a LOV domain (*10*, *18*, *20*, *21*, *34*, *45*, *46*). In LOV2 (404−546) this conserved glutamine, Gln513, is located on the Iβ strand, whose residues Ile510, Gly511, Val512, and Leu514 supply hydrophobic docking sites for the Jα helix (Figure 2B). Light-induced covalent adduct formation in LOV2 (404−546) displaces Gln513 slightly out of the flavin pocket toward

the N-terminal turn-helix-turn motif. Similar light-dependent displacements of conserved glutamines were observed in *A. capillus-veneris* phy3 LOV2 (Gln1029) (*10*), *C. reinhardtii* LOV1 (Gln120) (*18*), and *Neurospora crassa* Vivid (Gln182) (*34*). To maintain the hydrogen bond with the newly protonated N5 atom of the FMN after covalent adduct formation, it was proposed that these glutamine residues must flip their amide side chains. There is no direct, high-resolution structural evidence of such a flip. However, it could occur in the alternative conformation of Gln513 observed in RLS (Figure 3D). After such a flip, glutamines make also new hydrogen bonds with adjacent amino acid residues (*10*, *18*, *34*). Formation of the flavin−cysteinyl adduct drives breakage of a hydrogen bond between Asn414 and Asp515. The asparagine side chain then flips via rotation at its Cβ atom bringing the Asp414-Oδ1 atom within hydrogen-bond distance of the Gln513-Oϵ1 atom (Figure 3, parts C and D). The flipped side chain of Gln513 makes a new hydrogen bond with Asp414. That is, local, light-induced rearrangement of hydrogen bonds around the FMN contributes to displacement of the N-terminal flanking region and perhaps of the Jα helix (see below), i.e., to propagation of the structural signal to the surface of the protein.

Propagation of Structural Signal from the FMN to the Surface of Oat LOV2 (404−546). This direction of propagation in LOV2 (404−546) is similar to those seen in photoactive yellow protein (*41*, *42*) and the *Neurospora crassa* photoreceptor Vivid (*34*) but differs from that proposed for phy3 LOV2 (*47*). These differences may be influenced by the existence of flanking regions and crystal packing. The N-terminal turn-helix-turn motif and the two ends of the Jα helix make some intermolecular contacts (Figure 4A). Nevertheless, some atomic displacements do occur around residues Lys533 through Ile539 for which intermolecular contacts are absent (Figure 4, parts A and B). Remarkably, the importance of this middle part of the helix for signal propagation was also demonstrated by site-directed mutagenesis (*21*, *46*). The point mutations Ile532Glu, Ala536Glu, and Ile539Glu in oat LOV2 (404−560) and Ile608Glu in *A. thaliana* LOV2 disrupt the interactions between the Jα helix and the core domain and facilitate unfolding of the Jα helix and activation of the kinase domain. That is, these results and our crystallographic data identify the importance of the Jα helix in signal transduction. However, this helix may not be the sole contributor to signal transduction: the most prominent structural changes that we have observed in a crystalline lattice do occur on the surface of the protein next to the A′α−Aβ loop, Aβ strand, and Iβ strand.

ACKNOWLEDGMENT

We thank Dr. Vukica Šrajer and the staff of the 14-BM-C beamline, BioCARS, APS, for their assistance during data collection and microspectrophotometer measurements. The *A. sativa* LOV2 (404−560) construct and coordinates of its NMR dark structure were kindly provided by Dr. Kevin Gardner from the University of Texas Southwestern Medical Center. The LOV2 (404−546) construct was designed and cloned by John Wojcik from the University of Chicago. We thank Dr. Tobin Sosnick and Devin Strickland from the University of Chicago for sharing facilities for spectroscopic studies on LOV2 constructs in solution. We thank Vukica Šrajer, Andreas Möglich, Emina Stojković, Xiaojing Yang, and Rebecca Ayers for helpful discussions.

SUPPORTING INFORMATION AVAILABLE

One table and four figures that supplement results presented in the manuscript. This material is available free of charge via the Internet at http://pubs.acs.org.

REFERENCES

1. Briggs, W. R., Christie, J. M., and Salomon, M. (2001) Phototropins: A new family of flavin-binding photoreceptors in plants, *Antioxid. Redox Signaling 3*, 775−788.
2. Briggs, W. R., Beck, C. F., Cashmore, A. R., Christie, J. M., Hughes, J., Jarillo, J. A., Kagawa, T., Kanegae, H., Liscum, E., Nagatani, A., Okada, K., Salomon, M., Rüdiger, W., Sakai, T., Takano, M., Wada, M., and Watson, J. C. (2001) The phototropin family of photoreceptors, *Plant Cell 13*, 993−997.
3. Sakai, T., Kagawa, T., Kasahara, M., Swartz, T., Christie, J., Briggs, W., Wada, M., and Okada, K. (2001) Arabidopsis nph1 and npl1: Blue-light receptors that mediate both phototropism and chloroplast relocation, *Proc. Natl. Acad. Sci. U.S.A. 98*, 6969−6974.
4. Kinoshita, T., Doi, M., Suetsugu, N., Kagawa, T., Wada, M., and Shimazaki, K. (2001) Phot1 and phot2 mediate blue light regulation of stomatal opening, *Nature 414*, 656−660.
5. Sakamoto, K., and Briggs, W. R. (2002) Cellular and subcellular localization of phototropin 1, *Plant Cell 14*, 1723−1735.
6. Briggs, W., and Christie, J. (2002) Phototropins 1 and 2: Two versatile plant blue-light receptors, *Trends Plant Sci. 7*, 204−210.
7. Christie, J. M., Reymond, P., Powell, G. K., Bernasconi, P., Raibekas, A. A., Liscum, E., and Briggs, W. R. (1998) Arabidopsis NPH1: A flavoprotein with the properties of a photoreceptor for phototropism, *Science 282*, 1698−1701.
8. Christie, J. M., Salomon, M., Nozue, K., Wada, M., and Briggs, W. R. (1999) LOV (light, oxygen, or voltage) domains of the blue-light photoreceptor phototropin (nph1): Binding sites for the chromophore flavin mononucleotide, *Proc. Natl. Acad. Sci. U.S.A. 96*, 8779−8783.
9. Taylor, B. L., and Zhulin, I. B. (1999) PAS domains: internal sensors of oxygen, redox potential and light, *Microbiol. Mol. Biol. Rev. 63*, 479−506.
10. Crosson, S., and Moffat, K. (2002) Photoexcited structure of a plant photoreceptor domain reveals a light-driven molecular switch, *Plant Cell 14*, 1067−1075.
11. Swartz, T. E., Wenzel, P. J., Corchnoy, S. B., Briggs, W. R., and Bogomolni, R. A. (2002) Vibration spectroscopy reveals light-induced chromophore and protein structural changes in the LOV2 domain of the plant blue-light receptor phototropin 1, *Biochemistry 41*, 7183−7189.
12. Salomon, M., Christie, J. M., Knieb, E., Lempert, U., and Briggs, W. R. (2000) Photochemical and mutational analysis of the FMN binding domains of the plant blue light receptor, phototropin, *Biochemistry 39*, 9401−9410.
13. Salomon, M., Eisenreich, W., Durr, H., Schleicher, E., Knieb, E., Massey, V., Rudiger, W., Muller, F., Bacher, A., and Richter, G. (2001) An optomechanical transducer in the blue light receptor phototropin from Avena sativa, *Proc. Natl. Acad. Sci. U.S.A. 98*, 12357−12361.
14. Christie, J. M., Swartz, T. E., Bogomolni, R. A., and Briggs, W. R. (2002) Phototropin LOV domains exhibit distinct roles in regulating photoreceptor function, *Plant J. 32*, 205−219.
15. Salomon, M., Lempert, U., and Rüdiger, W. (2004) Dimerization of the plant photoreceptor phototropin is probably mediated by the LOV1 domain, *FEBS Lett. 572*, 8−10.
16. Liscum, E., and Stowe-Evans, E. L. (2000) Phototropism: a "simple" physiological response modulated by multiple interacting photosensory-response pathways, *Photochem. Photobiol. 72*, 273−282.
17. Crosson, S., and Moffat, K. (2001) Structure of a flavin-binding plant photoreceptor domain: Insights into light-mediated signal transduction, *Proc. Natl. Acad. Sci. U.S.A. 98*, 6969−6974.
18. Fedorov, R., Schlichting, I., Hartmann, E., Domratcheva, T., Fuhrmann, M., and Hegemann, P. (2003) Crystal structures and molecular mechanism of a light induced signaling switch: the

Phot-LOV1 domain from Chlamydomonas reinhardtii, *Biophys. J. 84*, 2474−2482.
19. Corchnoy, S. B., Swartz, T. E., Lewis, J. W., Szundi, I., Briggs, W. R., and Bogomolni, R. A. (2003) Intramolecular proton transfers and structural changes during the photocycle of the LOV2 domain of phototropin 1, *J. Biol. Chem. 278*, 724−731.
20. Harper, S. M., Neil, L. C., and Gardner, K. H. (2003) Structural basis of a phototropin light switch, *Science 301*, 1541−1544.
21. Harper, S. M., Christie, J. M., and Gardner, K. H. (2004) Disruption of the LOV-J helix interaction activates phototropin kinase activity, *Biochemistry 43*, 16184−16192.
22. Chen, Y., Šrajer, V., Ng, K., Legrand, A., and Moffat, K. (1994) Optical monitoring of protein crystals in time-resolved X-ray experiments: Microspectrophotometer design and performance, *Rev. Sci. Instrum. 65*, 1506−1511.
23. Otwinowski, Z., and Minor, W. (1997) Processing of X-ray data diffraction data collected in oscillation mode, *Methods Enzymol. 276*, 307−326.
24. Navaza, J. (1994) AMoRe: An automated package for molecular replacement, *Acta Crystallogr. A50*, 157−163.
25. Emsley, P., and Cowtan, K. (2004) Coot: model-building tools for molecular graphics, *Acta Crystallogr. D60*, 2126−2132.
26. Murshudov, G. N., Vagin, A. A., and Dodson, E. J. (1997) Refinement of macromolecular structures by the maximum-likelihood method, *Acta Crystallogr. D53*, 240−255.
27. Laskowski, R. A., MacArthur, M. W., Moss, D. S., and Thornton, J. M. (1993) PROCHECK: a program to check the stereochemical quality of protein structures, *J. Appl. Crystallogr. 26*, 283−291.
28. Morris, A. L., MacArthur, M. W., Hutchinson, E. G., and Thornton, J. M. (1992) Stereochemical quality of protein structure coordinates, *Proteins 12*, 345−364.
29. Hooft, R. W. W., Vriend, G., Sander, C., and Abola, E. E. (1996) Errors in protein structures, *Nature 381*, 272−272.
30. Kabsch, W. (1976) A solution for the best rotation to relate two sets of vectors, *Acta Crystallogr. A32*, 922−923.
31. Holm, L., and Park, J. (2000) DaliLite workbench for protein structure comparison, *Bioinformatics 16*, 566−567.
32. Potterton, E., Briggs, P., Turkenburg, M., and Dodson, E. (2003) A graphical user interface to the CCP4 program suite, *Acta Crystallogr. D59*, 1131−1137.
33. Swartz, T. E., Corchnoy, S. B., Christie, J. M., Lewis, J. W., Szundi, I., Briggs, W. R., and Bogomolni, R. A. (2001) The photocycle of a flavin-binding domain of the blue light photoreceptor phototropin, *J. Biol. Chem. 276*, 36493−36500.
34. Zoltowski, B. D., Schwerdtfeger, C., Widom, J., Loros, J. J., Bilwes, A. M., Dunlap, J. C., and Crane, B. R. (2007) Conformational switching in the fungal light sensor Vivid, *Science 316*, 1054−1057.
35. Key, J., Hefti, M., Purcell, E. B., and Moffat, K. (2007) Structure of the redox sensor domain of *Azotobacter vinelandii* NifL at atomic resolution: Signaling, dimerization, and mechanism, *Biochemistry 46*, 3614−3623.
36. Key, J., and Moffat, K. (2005) Crystal structure of deoxy and CO-bound bjFixLH reveal details of ligand recognition and signaling, *Biochemistry 44*, 4627−4635.
37. Kurokawa, H., Lee, D. S., Watanabe, M., Sagami, I., Mikami, B., Raman, C. S., and Shimizu, T. (2004) A redox-controlled molecular switch revealed by the crystal structure of a bacterial heme PAS sensor, *J. Biol. Chem. 279*, 20186−20193.
38. Miyatake, H., Mukai, M., Park, S. Y., Adachi, S., Tamura, K., Nakamura, H., Nakamura, K., Tsuchiya, T., Iizuka, T., and Shiro, Y. (2000) Sensory mechanism of sensor FixL from *Rhizobium meliloti*: Crystallographic, mutagenesis and resonance Raman spectroscopic studies, *J. Mol. Biol. 301*, 415−431.
39. Park, H., Suquet, C., Satterlee, J. D., and Kang, C. (2004) Insights into signal transduction involving PAS domain oxygen-sensing heme proteins from the X-ray crystal structure of *Escherichia coli* Dos heme domain (Ec DosH), *Biochemistry 43*, 2738−2746.
40. Anderson, S., Crosson, S., and Moffat, K. (2004) Short hydrogen bonds in photoactive yellow protein, *Acta Crystallogr. D60*, 1008−1016.
41. Anderson, S., Šrajer, V., Pahl, R., Rajagopal, S., Schotte, F., Anfinrud, P., Wulff, M., and Moffat, K. (2004) Chromophore conformation and the evolution of tertiary structural changes in photoactive yellow protein, *Structure 12*, 1039−1045.
42. Ihee, H., Rajagopal, S., Šrajer, V., Pahl, R., Anderson, S., Schmidt, M., Schotte, F., Anfinrud, P. A., Wulff, M., and Moffat, K. (2005) Visualizing reaction pathways in photoactive yellow protein from nanoseconds to seconds, *Proc. Natl. Acad. Sci. U.S.A. 102*, 7145−7150.
43. Cho, H-Y., Tseng, T-S., Kaiserli, E., Sullivan, S., Christie, J. M., and Briggs, W. R. (2007) Physiological roles of the light, oxygen, or voltage domains of phototropin 1 and phototropin 2 in *Arabidopsis*, *Plant Physiol. 143*, 517−529.
44. Chen, E., Swartz, T. E., Bogomolni, R. A., and Kliger, D. S. (2007) A LOV story: The signaling state of the phot1 LOV2 photocycle involves chromophore-triggered protein structure relaxation, as probed by far-UV time-resolved optical rotatory dispersion spectroscopy, *Biochemistry 46*, 4619−4624.
45. Nozaki, D., Iwata, T., Ishikawa, T., Todo, T., Tokutomi, S., and Kandori, H. (2004) Role of Gln1029 in the photoactivation process of the LOV2 domain in *Adiantum* phytochrome3, *Biochemistry 43*, 8373−8379.
46. Jones, M. A., Feeney, K. A., Kelly, S. M., and Christie, J. M. (2006) Mutational analysis of phototropin 1 provides insights into the mechanism underlying LOV2 signal transmission, *J. Biol. Chem. 282*, 6405−6414.
47. Crosson, S., Rajagopal, S., and Moffat, K. (2003) The LOV domain family: Photoresponsive signaling modules coupled to diverse output domains, *Biochemistry 42*, 2−10.
48. DeLano, W. L. (2002) The PyMOL Molecular Graphics System, DeLano Scientific, Palo Alto, CA, U.S.A., available at http://www.pymol.org.
49. Altschul, S. F., Madden, T. L., Schäffer, A. A., Zhang, J., Zhang, Z., Miller, W., and Lipman, D. J. (1997) Gapped BLAST and PSI-BLAST: a new generation of protein database search programs, *Nucleic Acids Res. 25*, 3389−3402.
50. Hall, T. A. (1999) BioEdit: a user-friendly biological sequence alignment editor and analysis program for Windows 95/98/NT, *Nucleic Acids Symp. Ser. 41*, 95−98.
51. Chenna, R., Sugawara, H., Koike, T., Lopez, R., Gibson, T. J., Higgins, D. G., and Thompson, J. D. (2003) Multiple sequence alignment with the Clustal series of programs, *Nucleic Acids Res. 31*, 3497−3500.
52. Koradi, R., Billeter, M., and Wüthrich, K. (1996) MOLMOL: a program for display and analysis of macromolecular structures, *J. Mol. Graphics 14*, 51−55.

BI701543E